Convective heat transfer performance of thermal oil-based nanofluids in a high-temperature thermohydraulic loop

Javier Gil-Font, Nuria Navarrete, Estefanía Cervantes, Rosa Mondragón, Salvador F. Torró, Raúl Martínez-Cuenca, Leonor Hernández [*]

Departamento de Ingeniería Mecánica y Construcción, Universitat Jaume I, 12071, Castellón de La Plana, Spain

A B S T R A C T

Enhancing the performance of heat transfer fluids (HTF) is a key target for improving the efficiency of many industrial processes. Employing nanofluids for this purpose, by dispersing nanoparticles into the initial HTF to improve its thermo-physical properties, is one possible way to increase its heat transfer capacity. However, testing these properties at high temperature is not always easy. An experimental setup consisting of a thermo-hydraulic loop for high-temperature heat transfer measurements was developed in this work. The accuracy and repeatability of the measurements taken in the heat transfer loop were ensured. A nanofluid consisting of a commercial thermal oil, doped with Sn nanoparticles at 1 wt% and olive oil surfactant used to enhance colloidal stability, was tested and compared to the results obtained for the base fluid and the base fluid/stabiliser mixture employing their experimentally measured thermo-physical properties. The nanofluid generally enhanced the convective heat transfer coefficient in relation to the base fluid with enhancements of up to 7.23% at 200 °C and 9.43% at 140 °C *vs.* the pure base fluid.

1. Introduction

The number of processes that involve heat transfer in the world today is outstanding, and range from chemical or oil/gas industries to the solar thermal energy sector, including the cooling of electronic devices, chemical and nuclear reactors, engines, etc. This is one of the reasons why the heat transfer fluids (HTFs) market is expected to continue to grow in forthcoming years [1,2].

In order to reduce the costs associated with these processes, heat transfer efficiency needs to be enhanced, and must allow smaller and more cost-effective installations and devices. Single-phase convective heat transfer depends mainly on the thermo-physical properties and velocity of HTFs and the system's geometry. Therefore, the approaches followed to enhance the efficiency of heat transfer processes have traditionally involved increasing flow velocity, altering the system's geometry to make a larger exchange surface available (e.g. increasing the roughness of piping) [3,4] or modifying HTFs. This work dealt with the latter alternative, and research was conducted to modify the thermo-physical properties of HTFs. This is especially relevant for the HTFs used at high working temperatures, whose thermal properties are not as good compared to, for example, those of water. Therefore,

enhancing heat transfer by modifying HTFs can be achieved by directly replacing the working fluid with a more suitable one, which is not always easy, or by adding dispersed particles to the original fluid to create what is known as a nanofluid [5,6].

Nanofluids are stable colloidal suspensions of particles with a size range of 10–100 nm. The term was first coined by Choi in 1995 [7], although Masuda et al. had previously used a suspension of nanoparticles to enhance thermal conductivity [8]. The addition of solid particles to a fluid allows, to a certain extent, the thermo-physical properties of a solid to be introduced into liquid and, therefore, the enhancement of the thermal conductivity of HTFs should be possible. The main advantage of nanofluids over suspensions of micron- or millimetre-sized particles is that they can form homogeneous dispersions that minimise channel abrasion or clogging problems. However, it can be argued that the addition of nanoparticles can negatively affect other thermo-physical properties of fluids, e.g. increasing their viscosity and density, or reducing their specific heat [9–11]. Although theoretical models and correlations are found in the literature to predict these properties, experimental determination is more widely accepted for some of them to avoid controversy [12].

In order to determine a fluid's heat transfer performance, the convective heat transfer coefficient (h) is widely used. It can be

Nomenclature

HTF	Heat transfer fluid
RTD	Resistance temperature detector
OO	Olive oil
Sn	Tin
TH66	Therminol 66

Symbols

c_p	Specific heat
d	Inner pipe diameter
D	Outer pipe diameter
e	Emissivity
ε	Pipe wall roughness
E	Error
f	Darcy friction factor
h	Convective heat transfer coefficient
k	Thermal conductivity
L	Pipe length
μ	Dynamic viscosity
Mo	Mouromtseff number
Nu	Nusselt number
Pr	Prandtl number
q	Heat power flux

q'	Linear heat power flux
Q	Volumetric flow rate
Re	Reynolds number
ρ	Density
σ	Stefan-Boltzmann constant
S	Standard deviation
T	Temperature
z	Axial position

Subscripts

amb	Ambient
ave	Average temperature
bf	Base fluid
$calibration$	Calibration test
$corr$	Correlation
exp	Experimental
f	Fluid
in	Inner
$measured$	Experimentally measured
nf	Nanofluid
out	Outer
rad	Radiation
w	Wall

theoretically determined by means of Nusselt (Nu) number correlations or figures of merit like the Mouromtseff (Mo) number [13,14], and also experimentally by an experimental setup consisting of a thermohydraulic loop that emulates on the lab scale the conditions that would be met in a real installation. This kind of apparatus can offer reliable data on the behaviour of an HTF under specific working conditions as regards its convective heat transfer coefficient.

The experimental determination of a fluid's convective heat transfer capacity at temperatures above 50 °C is more frequent in the literature for nanofluids based on water [15–19] or glycol, and water mixtures [20–25]. Many works have studied the thermo-physical properties of oil-based nanofluids [26], but only a few have experimentally measured the convective heat transfer coefficient [27–36]. Moreover, research into this type of installations to measure convective heat transfer co-efficients of fluids above 100 °C is scarce. A few works have measured heat transfer experimentally using thermal oils [37,38] or molten salts [39–43] as HTFs. Table 1 summarises the works that have used a thermohydraulic loop for nanofluids at temperatures exceeding 50 °C, and HTFs without nanoparticles at temperatures over 100 °C. To the best of our knowledge, no works that have experimentally measured the convective heat transfer coefficient for nanofluids at high temperatures are available in the literature. The nature of the studied fluids, the tested temperature range and the type of nanoparticles used with nanofluids are indicated, as is the way the thermo-physical properties needed for the convective heat transfer coefficient calculation are determined, which can be experimentally or theoretically (using models and correlations from the literature or those provided by fluid suppliers).

To be able to experimentally determine the heat transfer coefficient using a thermohydraulic loop, the thermo-physical properties of the tested fluid (viscosity, thermal conductivity, specific heat, density) play a key role. Alterations to these properties when adding nanoparticles to a base fluid are a questioned topic in the literature, and many correlations have been made to predict them [11,44], but they are often very specific for a given base fluid and nanoparticle combination or experimental conditions. So even though specific heat and density are frequently well predicted with theoretical correlations based on the mixture rule [12], the experimental determination of other nanofluid thermo-physical properties (especially thermal conductivity and

viscosity) is a more reliable method. However, as the last column of Table 1 suggests, either theoretical models or correlations of these properties are used for convective heat transfer coefficient calculations in many published papers.

In this article, and to the best of the authors' knowledge, a setup consisting of a high-temperature thermohydraulic loop (up to 200 °C) was constructed for the first time for the experimental determination of the convective heat transfer coefficient of HTFs, and a thermal oil-based nanofluid and base fluids were tested. The nanofluid employed in this research was produced, stabilised and characterised at high temperature in a previous work [45], and is composed of thermal oil Therminol 66 (TH66), olive oil (OO) as a colloidal stabiliser and Sn nanoparticles at a 1 wt% concentration. The convective heat transfer coefficients of the three fluids under study (base Therminol 66, Therminol 66 with OO as a stabiliser and the nanofluid) were experimentally measured in the high-temperature thermohydraulic loop within a range from 80 °C to 200 °C. The experimental results were compared to those predicted with the theoretical correlations to determine the Nusselt number. In all cases, the experimental thermo-physical properties (viscosity, thermal conductivity, specific heat) measured at high temperature were utilised because theoretical predictions might not come close to the actual values. Additionally, from the convective heat transfer coefficients experimentally obtained in the loop, the heat transfer enhancements recorded for the nanofluid in relation to the base fluid were evaluated.

2. Experimental section

2.1. Nanofluid characteristics

The fluids tested in this work were produced and characterised at high temperature in a previous work together with a thorough size and morphological characterisation of nanoparticles [45]. Synthetic commercial thermal oil (Therminol 66, Solution Inc.) was used as the base fluid. Olive oil was added as a stabiliser capable of withstanding the thermal oil working temperatures. Sn nanoparticles, with a nominal size of <300 nm (US Research Nanomaterials, Inc.), were dispersed in thermal oil. To produce the nanofluid, a concentration of 0.025 ml of OO per gram of Therminol 66 and 1 wt% of nanoparticles proved optimal in

Table 1

Literature review on the experimental measurement of the heat transfer of nanofluids above 50 °C and heat transfer fluids without nanoparticles above 100 °C.

Ref.	Base Fluid	Nanoparticles	Temp. Range	Thermo-physical properties determination
[15]	Water	Al_2O_3	45–65 °C	Theoretical
[16]	Water	Al_2O_3, ZrO_2	21–76 °C	Theoretical (specific heat, density) and Experimental (thermal conductivity, viscosity)
[17]	Water	Al_2O_3, polystyrene, SiO_2	15–78 °C	Theoretical (specific heat) and Experimental (thermal conductivity, density, viscosity)
[18]	Water	Al_2O_3	60–94 °C	Theoretical
[19]	Water	Al_2O_3, CNTs, SiO_2	40-80 °C	Theoretical (density) and Experimental (thermal conductivity, specific heat, viscosity)
[24]	EG	Al_2O_3, CuO	45–75 °C	Theoretical
[27]	Base oil SN 500	CuO	N/A	Experimental
[28]	Base oil SN 500	CuO	N/A	Experimental
[29]	Diesel oil	MWCNT Graphene	N/A	Theoretical
[30]	Transformer oil	Al_2O_3	N/A	Theoretical
[31]	Turbine oil	MWCNT	N/A	Theoretical (specific heat, density) and Experimental (thermal conductivity, viscosity)
[32]	Turbine oil	Al_2O_3, CuO, TiO_2	45–65 °C	Theoretical
[33]	Automatic transmission fluid, Oil mixture	Graphite	50–70 °C	Experimental
[34]	Heat transfer oil (Iranol HTB)	MWCNT	25–90 °C	Experimental
[35]	Heat transfer oil	MWCNT	95 °C	Experimental
[36]	Turbine oil	TiO_2	20-100 °C	Theoretical
[37]	Heat transfer oil (Therminol VP-1)	–	50–200 °C	Theoretical (specific heat, thermal conductivity) and Experimental (viscosity, density)
[38]	Heat transfer oil (Thermia B)	–	100–200 °C	Theoretical
[39]	Molten salt (KNO_3–$NaNO_2$–$NaNO_3$)	–	220–350 °C	Experimental
[40]	Molten salt (KNO_3–$NaNO_2$–$NaNO_3$)	–	210–400 °C	Theoretical
[41]	Molten salt (KNO_3–$NaNO_2$–$NaNO_3$)	–	250–400 °C	Experimental
[42]	Molten salt ($LiNO_3$)	–	272–440 °C	Theoretical
[43]	Molten salt (KNO_3–$NaNO_2$–$NaNO_3$)	–	289–442 °C	Theoretical

terms of colloidal stability and thermal properties enhancement at high temperatures. A long process was followed to select tin nanoparticles, including a literature review of the metal and metal oxides in thermal oils, an analysis of the most relevant variables for heat transfer performance together with prices and, finally, an evaluation of the high-temperature stability of the resulting nanofluids with the pre-selected nanoparticles. Tin nanoparticles provided interesting high thermal conductivity and density values at a reasonable cost, and presented the best nanofluid stability evaluation results. These stability tests included a variety of concentrations of the different surfactants, a visual examination of samples after 24 h in an oven at 140 °C, and ended by selecting OO as the stabiliser and its optimum concentration [45].

In order to produce the nanofluid, the stabiliser (OO) was added to the base thermal oil (TH66) and the mixture was mechanically stirred. Then it was heated at 80 °C and Sn nanoparticles were added. Nanoparticle dispersion was achieved by applying sonication for 5 min using an ultrasound probe (Sonopuls HD2200, Bandelin, HF-output of 200 W and HF-frequency of 20 kHz), and by paying special attention to ensure that its temperature would not exceed 100 °C in line with the ultrasound probe's working temperature limit. For the experimentation in the heat transfer loop, 25 L of nanofluid were produced in 1-L aliquots following this procedure. Fig. 1 shows the different samples tested in the loop: base fluid (TH66), mixture of base fluid with surfactant (TH66 + OO) and nanofluid (TH66 + OO + Sn).

Fig. 2 summarises the thermo-physical properties measured experimentally for the base fluids and the nanofluid in Ref. [45], along with their corresponding experimental errors. Thermal conductivity, dynamic viscosity and specific heat were measured at 80 °C, 100 °C, 120 °C and 140 °C. The obtained data were fitted to second-degree polynomials or power functions to extrapolate their values up to 225 °C. The experimental errors, E, were obtained following the Student's t-distribution in Eq. (1) for a 95% confidence level and n-$1°$ of freedom:

$$E = t_{n-1,0.025}\frac{S}{\sqrt{n}} \tag{1}$$

where S is the standard deviation of the n measurements taken. The average values of these experimental errors were 1.81%, 0.59% and 1.07% for thermal conductivity, viscosity and specific heat measurements, respectively.

Density values were calculated using the mixture rule equation. More details can be found in Ref. [45].

2.2. Experimental setup

The experimental apparatus used in this work is depicted schematically in Fig. 3a) and also shown in Fig. 4a). It consisted of a
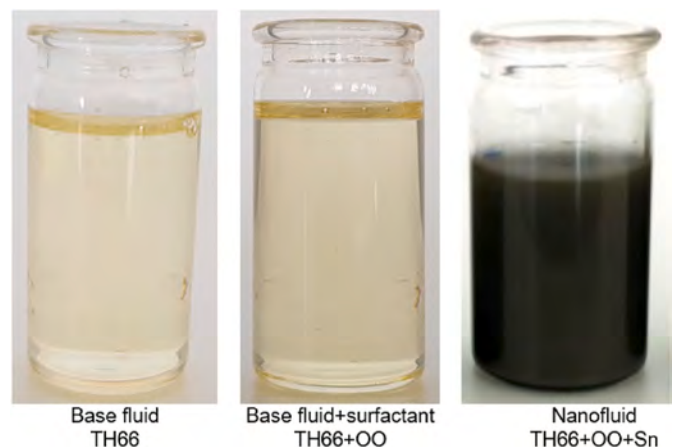

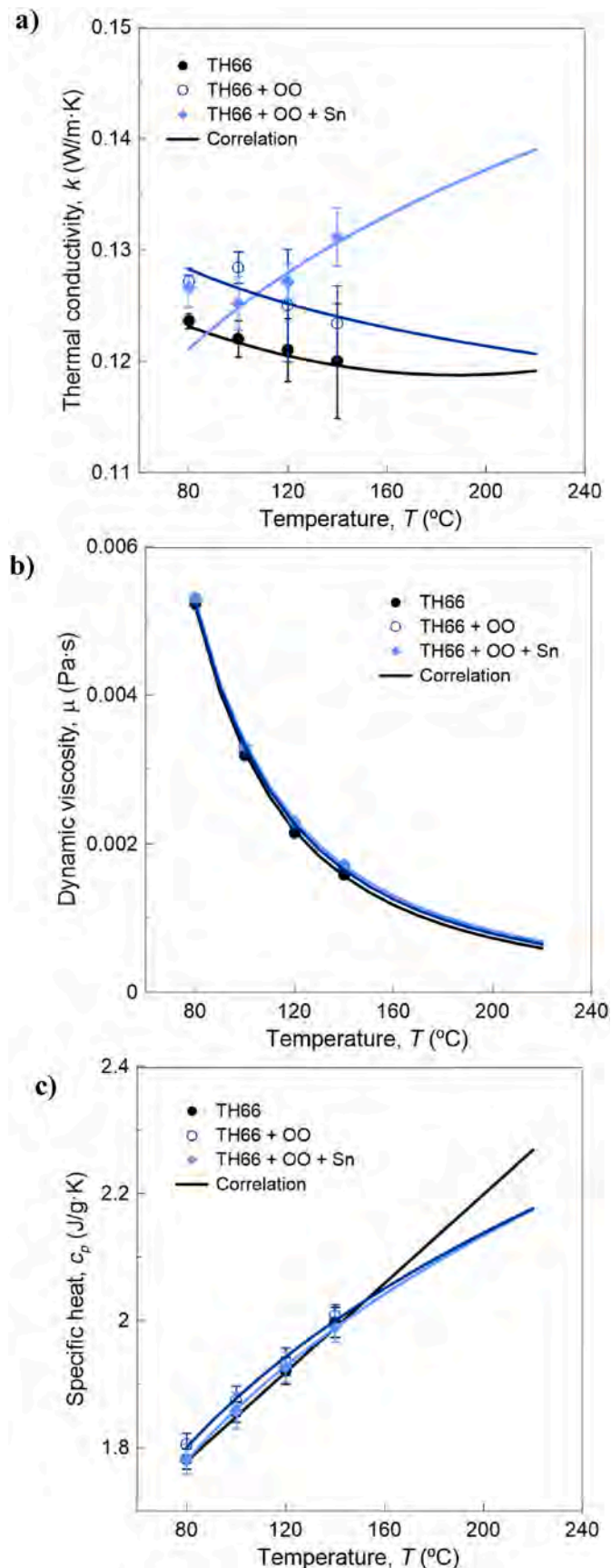**Fig. 1.** The base fluid, base fluid + surfactant and nanofluid samples.

Fig. 2. a) Thermal conductivity, b) dynamic viscosity and c) specific heat of the base fluids (TH66 and TH66 + OO) and the nanofluid (TH66 + OO + Sn). Experimental values: data points; correlations: continuous line.

thermohydraulic loop designed for high-temperature fluids. It comprised a main tank that can store up to 100 L (minimum of 25 L under working conditions) where fluid was stored. A centrifugal pump (SIHI SuperNova ZTN-032160) was selected especially for heat transfer oils and used to move the fluid to a test section. The combined use of a centrifugal pump and a bypass controlled by a globe valve finely adjusted the flow rate, which was measured by a flowmeter (RAMC, ROTA YOKOGAWA) with a maximum working temperature of 370 °C, a measurement range from 2 to 24 l/min and a measuring accuracy of 1.6% under the calibration conditions.

The test section consisted of a 2 m-long stainless steel 316 pipe with an inner diameter of 7 mm, an outer diameter of 10 mm, and 1.5 μm surface roughness. An electrical power source (EA-Elektro-Automatic EA-PSI 900 3U 10 kW, output voltage 0–80 V, output current 0–340 A) supplied current to the section, used to increase the fluid temperature due to the Joule effect. The output power of the electrical source was limited to 5 kW for safety reasons. In the test section, 10 resistance temperature detectors (RTDs) Pt100 with 1/3 DIN ($\pm$(0.1 + 0.5 %T)) tolerance were placed along the pipe to measure the temperature on its outer wall. Details of the positions of these RTDs in the test section are shown in Figs. 3b) and Fig. 4b). Two K-thermocouples were inserted into the pipes at the inlet and outlet of the test section to measure fluid temperature.

After going through the test section, the fluid flowed either to a cooling section to lower its temperature or to the main tank once again. Before reaching the main tank, the working fluid passed through a preheater (CVLC737C5, Watlow) to recover heat loss through the circuit and to increase the fluid temperature whenever needed. The whole setup was thermally isolated with mineral wool to minimise heat loss.

2.3. Experimental conditions

In the present work, the base thermal oil, the thermal oil with OO as a stabiliser and the nanofluid containing Sn nanoparticles at the 1 wt% concentration were tested in the thermohydraulic loop at several temperatures and for different Reynolds numbers to evaluate and compare their convective heat transfer performance. The experimental conditions used in these experiments were the following:

(1) the experimental Reynolds number of the tested fluids varied within the range of 2500–25000,
(2) the fluid velocity always fell within the 0.9–5.5 m/s range,
(3) the inlet temperatures of the fluid were initially selected as 80 °C, 100 °C, 120 °C, 140 °C and 200 °C, with a temperature difference between the inlet and outlet temperatures in the test section of 25 °C. According to the previous constant Reynolds number and velocity criteria requirements, slightly different temperature ranges were chosen for different fluids.

Repeatability of measurements meant performing some of the tests twice under the same turbulence and temperature conditions, and variations less than 3.6% were always obtained. The detailed results are shown in Section 4.1 in Table 2.

2.4. Temperature measurement

Two K-thermocouples with $\pm$1.5 °C accuracy (within a range from −40 to 1100 °C) were inserted at the inlet and outlet of the test section to measure fluid temperature. Thermocouples were calibrated with a temperature calibrator Isocal-6 Venus 2150 B (Isotech) filled with silicon oil BESSIL F-100. Sensors were verified by comparing to a standard calibration thermocouple at three different temperatures, including minimum, maximum and an intermediate temperature within the range tested in the thermohydraulic loop. Checks were made to corroborate if the difference between thermocouples and the standard was lower than the provided accuracy.
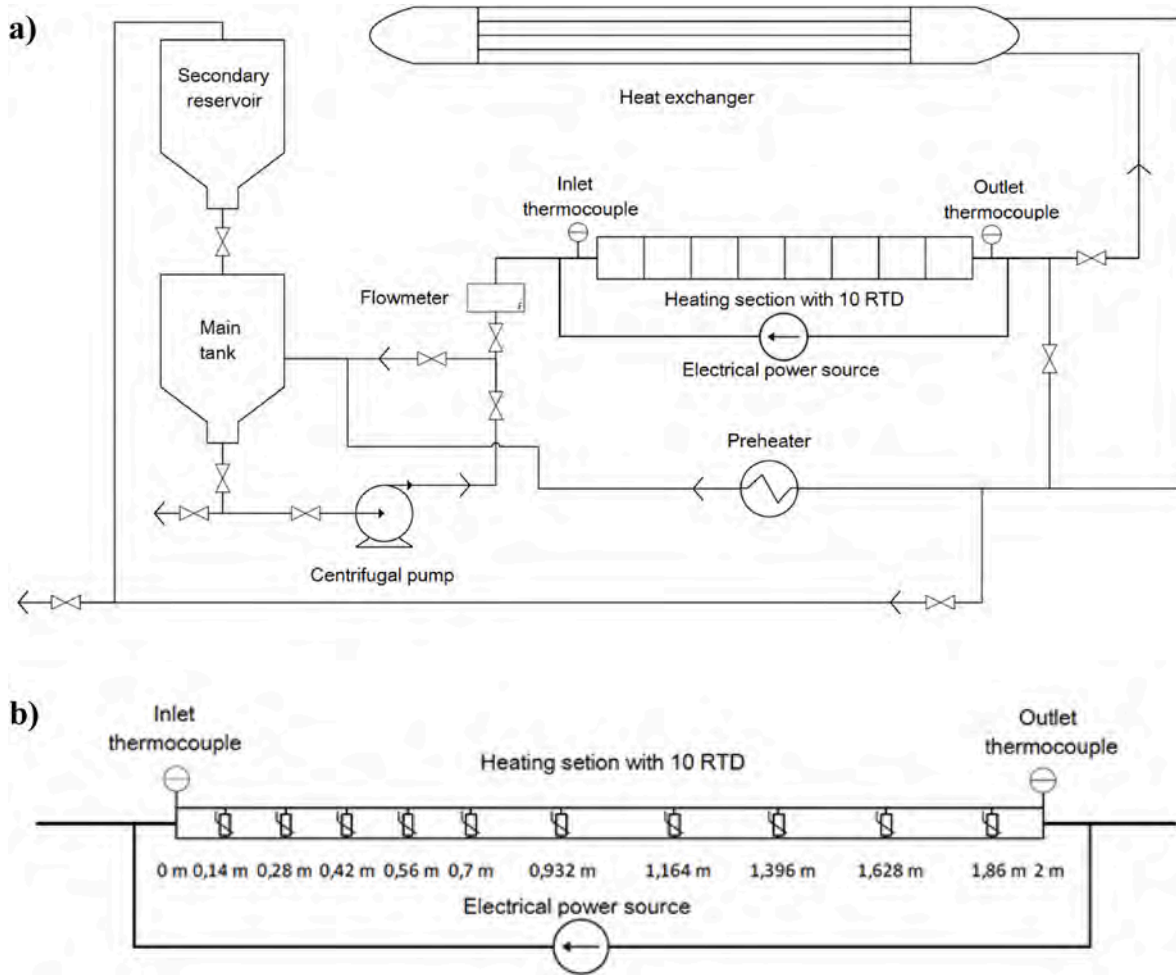
Fig. 3. Schematic view of the experimental setup. a) General view and b) detailed view of the test section.

Besides, 10 calibrated RTDs Pt100 temperature sensors with 1/3 DIN ($\pm(0.1 + 0.5\%T)$) tolerance and a measuring range from -50 to $500\ °C$ were placed on the pipe outer wall to determine their temperature. The axial position and distance between RTDs are indicated in Fig. 3b).

As the convective heat transfer coefficient measurement is very sensitive to differences in temperature, special care was taken in calibrating RTDs. To improve the reliability of temperature measurements, all the temperatures measured by sensors were corrected once they had been placed in their respective locations. To obtain the real outer wall temperature for each RTD placed in the z position, $T_{w,out}(z)$, a correction was done following Eq. (2):

$$T_{w,\ out}\ (z) = T_{w,out\_measured}\ (z)\ -\ RTD\ correction\ (z) \tag{2}$$

where $T_{w,out\_measured}$ is the wall temperature originally measured by the RTD and *RTD correction* is taken from a correction correlation obtained from a calibration test with TH66 under dynamic conditions, where fluid temperature was not constant. Starting at the highest wall temperature used in our tests, the fluid was then allowed to cool down without connecting the electrical power source, and flowed through the test section at a velocity close to 5 m/s. For each data acquisition instant, an average of all the 10 RTD measurements was calculated ($T_{ave,\ calibration}$). This procedure was repeated twice to obtain the temporal evolution curves of the fluid temperature with no significant differences. For each RTD, a correction correlation was determined based on the difference between the measured value ($T_{w,calibration}$) and the average ($T_{ave,\ calibration}$) at the same time in the calibration test, as shown in Eq. (3).

$$RTD\ correction\ (z) = T_{w,\ calibration}(z) - T_{ave,\ calibration} \tag{3}$$

Within the application range from $80\ °C$ to $200\ °C$, the minimum correction applied to any of the RTDs was 0.088% at $120\ °C$, the maximum was 2.21% at $200\ °C$, and the average correction for all the RTDs at all temperatures was 0.69%.

3. Convective heat transfer coefficient (h)

3.1. Experimental measurement

In order to obtain the convective heat transfer coefficient from the experimental measurements taken in the thermohydraulic loop at different z locations, $h(z)$, Eq. (4) was used:

$$h(z) = \frac{q(z)}{T_{w,in}(z) - T_f(z)} \tag{4}$$

where q is the heat power flow, $T_{w,in}$ is the local temperature of the pipe inner wall and T_f is the fluid's local temperature.

The heat power flux was determined from the energy balance in Eq. (5):

$$q(z) = \frac{\rho c_p Q}{\pi d L} \Delta T_f - q_{rad}(z) \tag{5}$$

where ρ, c_p and Q are the fluid density, fluid specific heat and volumetric flow rate respectively, and d and L are the inner diameter and pipe
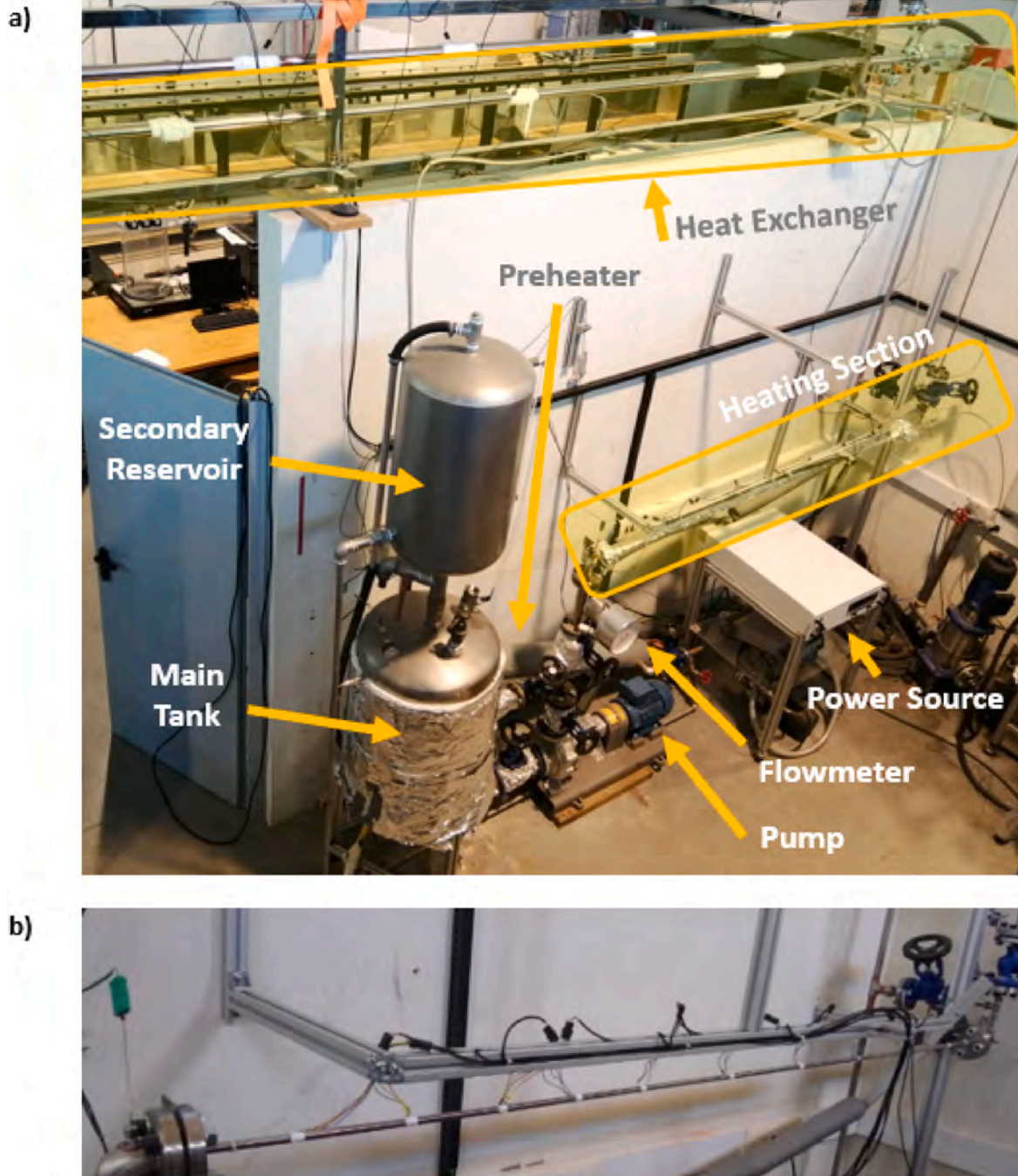
Fig. 4. Photographs of the different parts of the experimental setup. a) General photograph of the loop and b) a detailed photograph of the test section before being thermally isolated.

length in the test section respectively. ΔT_f is the difference between the inlet and outlet temperatures in the section and q_{rad} is the heat power flux emitted by radiation, which needs to be considered despite the setup isolation due to the high temperature differences reached between the wall temperature and the environment, as described by Eq. (6).

$$q_{rad}(z) = e\sigma\left(\left(T_{w,out}(z) + 273.15\right)^4 - \left(T_{amb} + 273.15\right)^4\right) \quad (6)$$

where e is the emissivity of the pipe material, σ is the Stefan-Boltzmann constant, and $T_{w,out}$ and T_{amb} are the temperatures in Celsius of the emitting body (the pipe outer wall) and the ambient temperature, respectively.

The local pipe inner wall temperature, $T_{w,in}(z)$, can be calculated

according to Eqs. (7) and (8) using the corrected values measured by the RTDs and some specific pipe parameters [46,47].

$$T_{w,in}(z) = T_{w,out}(z) + \frac{q'(z)}{4\,\pi\,k_{pipe}(z)} \frac{1 + \ln\left(\frac{d}{D}\right)^2 - \left(\frac{d}{D}\right)^2}{1 - \left(\frac{d}{D}\right)^2} \quad (7)$$

$$q'(z) = q(z)\cdot\pi\cdot d \quad (8)$$

where $T_{w,out}(z)$ is the local outer wall temperature in the test section (Eq. (2)) given by the RTDs and corrected as explained in Section 2.4, d and D are the inner and outer pipe diameters, respectively, k_{pipe} is its thermal

Table 2

Repeatability analysis of the experimental convective heat transfer coefficient.

Fluid	Temperature (°C)	Reynolds	h_1 (W/m^2·K)	h_2 (W/m^2·K)	h Difference (%)
TH66	80	4755	1284.36	1248.68	2.78
	100	6345	1626.45	1623.30	0.19
	120	3869	639.29	659.67	3.09
		7935	1851.69	1906.17	2.86
	140	11703	2526.83	2535.94	0.36
	200	20063	3600.67	3651.33	1.39
TH66 + OO	120	7901	1949.34	1940.43	0.46
	140	11475	2583.16	2638.89	2.11
	200	19159	3577.31	3591.35	0.39
TH66 + OO + Sn	100	8332	2240.53	2323.57	3.57
	120	7663	1891.87	1881.34	0.56
	140	7193	1584.47	1611.46	1.67
		10581	2477.68	2461.31	0.66
	200	18589	3509.41	3496.57	0.37

conductivity of the pipe material and q' is the linear heat flux emitted along the studied section.

Finally, to calculate the local temperature of the fluid at the position of each RTD, $T_f(z)$, Eq. (9) was used.

$$T_f(z) = \frac{z}{L}T_{f,out} + \left(1 - \frac{z}{L}\right)T_{f,in} \tag{9}$$

where z is the length in m where the RTD is placed, L is the total test section length, and $T_{f,out}$ and $T_{f,in}$ are the fluid temperatures at the test section outlet and inlet, respectively.

The convective heat transfer coefficient (h) was calculated by averaging the local heat transfer coefficients, $h(z)$, along the different z positions.

3.2. Theoretical modelling

The convective heat transfer coefficient (h) values were theoretically determined according to the Nusselt number (Nu) in Eq. (10):

$$Nu = \frac{h \cdot d}{k} \tag{10}$$

where d is the inner diameter of the test section and k is the thermal conductivity of the fluid.

For the turbulent flow regime, the Nusselt number depends on the Reynolds (Re) and Prandtl (Pr) numbers which, in turn, depend on thermal conductivity, specific heat and viscosity. From the correlations available in the literature, the Gnielinski correlation [48], valid within the Reynolds range 3000–5,000,000, proved suitable for predicting the convective heat transfer coefficient in nanofluids [19]:

$$Nu = \frac{f}{8}\frac{(Re - 1000)Pr}{1 + 12.7\sqrt{\frac{f}{8}}\left(Pr^{\frac{2}{3}} - 1\right)} \tag{11}$$

where f is the friction factor calculated by the Colebrook-White equation:

$$\frac{1}{\sqrt{f}} = -2 \cdot log\left[\frac{\varepsilon/d}{3.7} + \frac{2.51}{Re\sqrt{f}}\right] \tag{12}$$

where ε is the pipe's wall roughness.

Besides, the Dittus-Boelter correlation, valid within the Reynolds Re range >10,000, can be used to calculate the Nusselt number in the turbulent regime according to Eq. (13).

$$Nu = 0.023\,Re^{0.8} \cdot Pr^{0.4} \tag{13}$$

The Prandtl number was calculated for the base fluids and the nanofluid according to Eq. (14):

$$Pr = \frac{c_p\,\mu}{k} \tag{14}$$

where c_p is the specific heat, μ is dynamic viscosity and k is thermal conductivity of the working fluid.

4. Results and discussion

4.1. Thermohydraulic loop verification

Having constructed the thermohydraulic loop, the Nusselt number of base fluid Therminol 66 was experimentally obtained from the measurements taken in the loop as explained in the previous section. These data were compared to the most widely used theoretical correlations for turbulent heat transfer: Gnielinski and Dittus-Boelter [15–19,37–43]. For this analysis, the values of the thermo-physical properties (viscosity, specific heat, thermal conductivity, density) can be experimentally obtained as described in Section 2.1, or those provided by the supplier can be used. The experimental conditions measured in the loop covered five different inlet temperatures (80, 100, 120, 140 and 200 °C) and several Reynolds from 2500 to 25,000. The consistency of the data obtained from the measurements taken in the loop and those predicted by the Gnielinski and Dittus-Boelter correlations are found in Fig. 5, where the ratio between the experimental Nusselt numbers (Nu_{exp}) and the theoretical ones (Nu_{corr}) is plotted. Fig. 5a) shows the ratios of the Nusselt number calculated from the experimental values from the setup and correlations using the previously measured thermo-physical properties for different fluid temperatures and Reynolds numbers. The Nusselt number using the experimental loop data and the Gnielinski correlation with the measured properties were similar, with differences below 15%, except for the lowest Reynolds data, which came close to the lower validity limit of Gnielinski's equation. The data at 200 °C obtained differences close to 15%. The Dittus-Boelter correlation presented significantly wider divergence, especially at 200 °C. Fig. 5b) depicts a similar analysis for the Nusselt numbers predicted using the thermo-physical properties obtained from the base fluid technical data sheet [49]. As shown, the differences between the experimental values measured in the loop and the theoretical ones obtained from the correlations are higher than in the previous case Fig. 5a), which corroborates that using the experimental measurements of the thermo-physical properties for heat transfer determinations is recommended.

A similar analysis is depicted in Fig. 6a) and b) for the mixture of Therminol 66 with OO, and for the nanofluid composed of Therminol 66, OO and Sn nanoparticles, respectively, using only the experimentally measured thermo-physical properties (Section 2.1) because they offer more accurate results for both the Gnielinski and Dittus-Boelter correlations. In Fig. 6a), the relation between the loop results and the correlation results for the Therminol 66 and OO mixture is similar to that obtained for pure Therminol 66. For the flow regimes with a Reynolds number above 5000, the results well agree with the Gnielinski correlation with a 15% deviation, while the Dittus-Boelter correlation failed to match the experimental results at high temperature.

The similar analysis of the experimentally obtained nanofluid Nusselt numbers ratios and from the correlations in Fig. 6b) gave a better agreement between both values, especially for intermediate Reynolds number values. Once again, the larger discordances were obtained for Reynolds below 5000. In this nanofluid case, the experimental values obtained for the highest temperature (200 °C) much better agreed with both correlations, although Gnielinski still gave a better prediction.

A complete error analysis of the results presented in Figs. 5 and 6 can be found in the Supporting Information (Figs. S.1, S.2 and S.3), and obtained average errors of 2.56%, 2.02% and 1.81% for the ratios to the Gnielinski correlation of Therminol 66 (TH66), Therminol 66 with OO (TH66 + OO) and nanofluid (TH66 + OO + Sn), respectively, and of 2.09%, 1.97% and 1.16% for the same fluids compared to the Dittus-
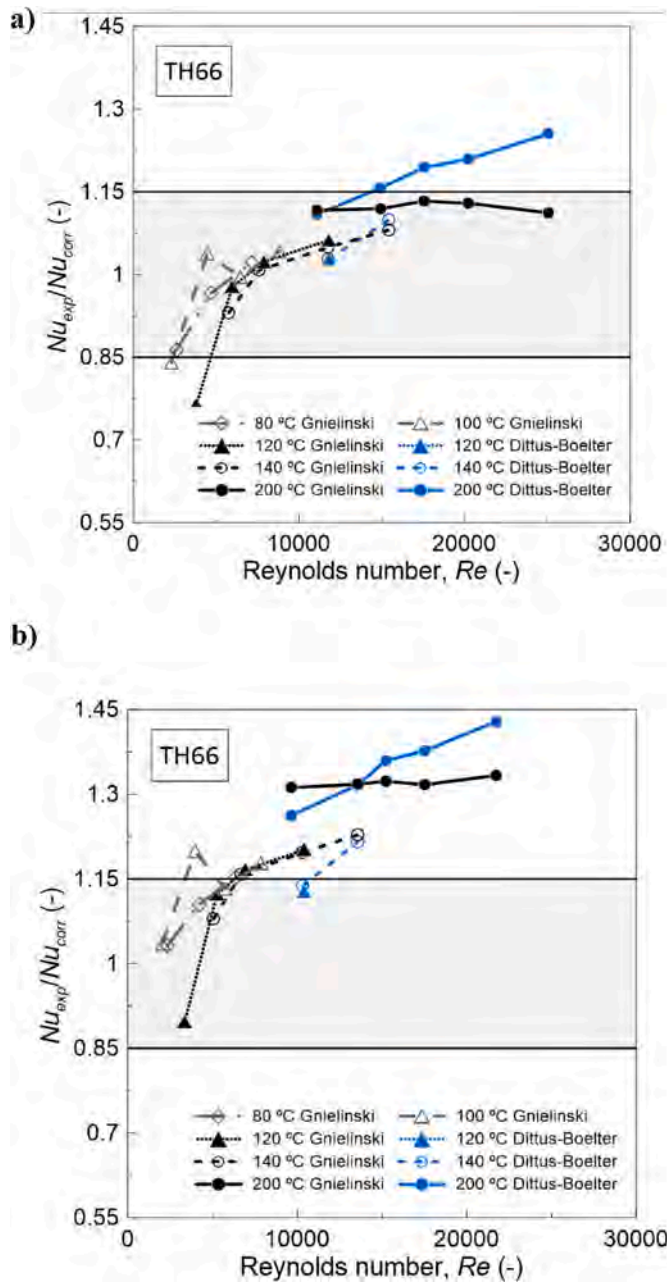
Fig. 5. Evolution with Reynolds and temperature of the Nusselt number ratios between the experimental and correlation values for Therminol 66. a) Thermo-physical properties experimentally measured and b) taken from the technical data sheet.

Fig. 6. Evolution with Reynolds and temperature of the Nusselt number ratios between the experimental and correlation values using the thermo-physical properties experimentally measured for a) base Therminol 66 with OO and b) nanofluid (TH66 + OO + Sn).

Boelter correlation.

In order to ensure the repeatability of the thermohydraulic loop results, tests were performed twice for some temperature conditions and Reynolds numbers. A summary of the obtained results is found in Table 2. For the base fluid, at least one test was repeated for each studied temperature. The differences obtained between measurements were always below 3.6%, which accounts for good repeatability. It is also worth highlighting the good repeatability of the nanofluid tests, with a mean error between the two heat transfer coefficient measurements of 1.37%. This also indicates good nanofluid stability with time when tested in the loop under real operating conditions.
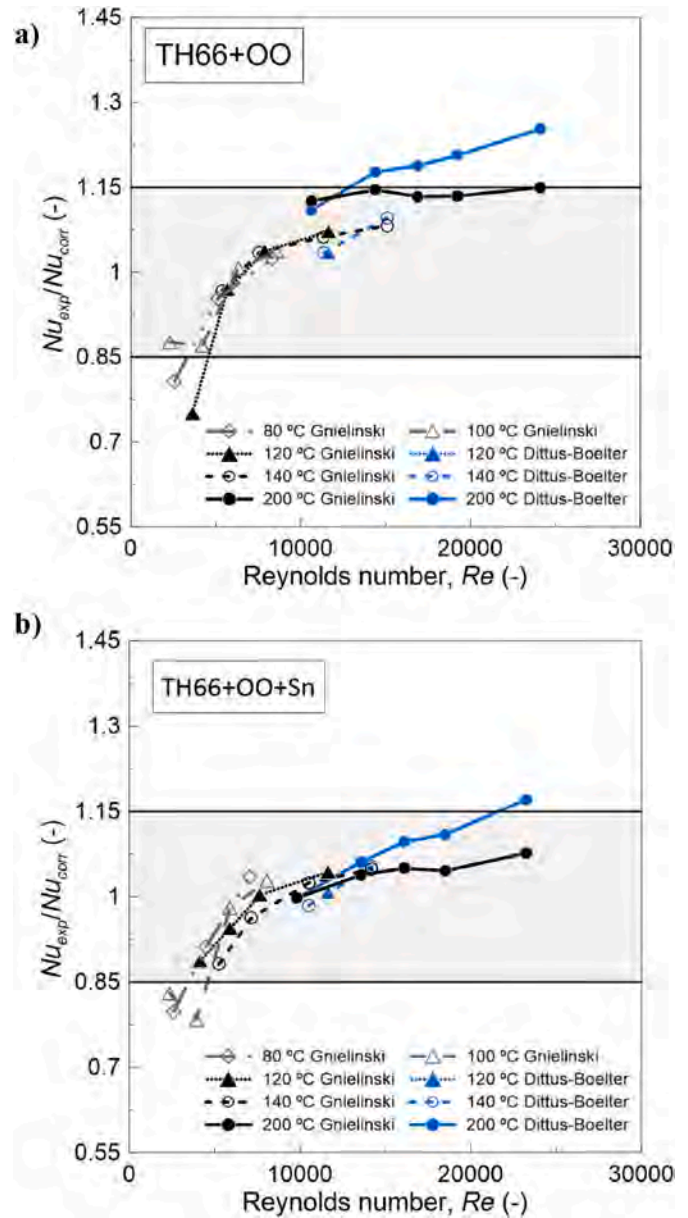
4.2. Nanofluid convective heat transfer coefficient enhancement

Having confirmed the accuracy of the data obtained from the thermohydraulic loop, the convective heat transfer coefficients of the base fluid, the base fluid with a stabiliser (OO) and nanofluid were determined. A comparison of the results obtained for the Therminol 66 and OO mixture and the nanofluid in relation to pure Therminol 66 is shown in Figs. 7 and 8.

The convective heat transfer coefficients obtained for the base fluid (TH66) and the base fluid with a stabiliser (TH66 + OO) are presented in Fig. 7 according to the Reynolds number for the different studied temperatures. For one same fluid, the convective heat transfer coefficient increased with Reynolds number, which was expected from the correlations and theoretical equations. When examining the influence of temperature for a constant Reynolds number, with increasing temperature, the reduction in the Prandtl number due to the main influence of
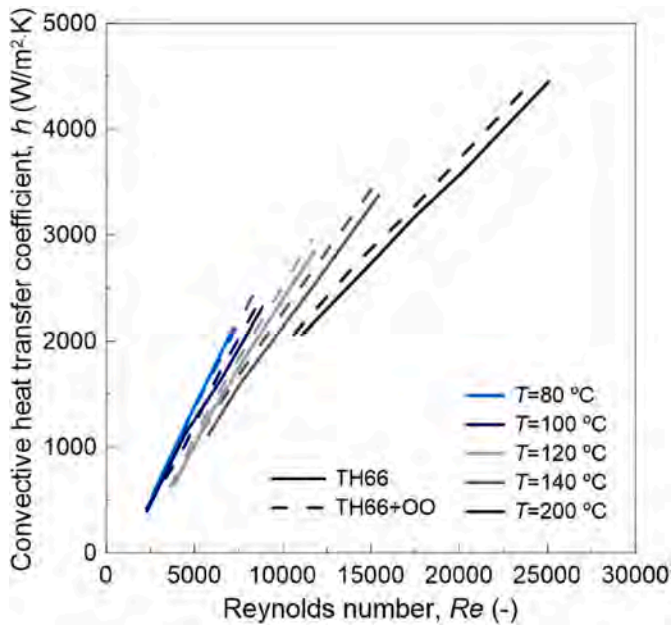
Fig. 7. Influence of Reynolds number and temperature on the convective heat transfer coefficient for Therminol 66 (TH66) and Therminol 66 with OO (TH66 + OO).
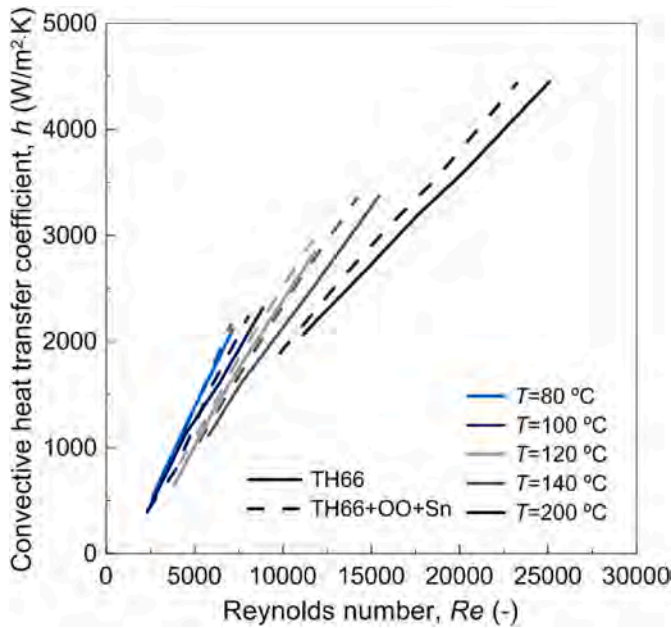

Fig. 8. Influence of Reynolds number and temperature on the convective heat transfer coefficient for Therminol 66 (TH66) and nanofluid (TH66 + OO + Sn).

decreased viscosity with temperature led to lower Nusselt values and, consequently, lower convective heat transfer coefficient values were obtained. The reduction in viscosity with temperature also impacted the obtained Reynolds number, which resulted in higher Reynolds numbers at higher temperatures for the same flow rate.

The base fluid and stabiliser mixture is also depicted in Fig. 7 as dashed lines. The same trends noted for the base fluid are seen, with lower convective heat transfer coefficients for lower temperatures/ Reynolds numbers. Moreover, the comparison made between the solid line (TH66) and dashed line (TH66 + OO) can be used to evaluate the effect produced by adding a stabiliser. The results obtained for both the tested fluids were similar for the studied lower temperature/Reynolds

numbers. However, at higher temperatures/Reynolds numbers, adding a stabiliser to the base fluid slightly improved the heat transfer coefficient values, which could be accounted for by the slight improvement caused by OO in the thermo-physical properties, such as specific heat.

A similar comparison between the convective heat transfer coefficient of the base fluid (TH66) and the nanofluid composed of Therminol 66, OO and Sn nanoparticles (TH66 + OO + Sn) is depicted in Fig. 8. According to the results obtained for the nanofluid (dashed lines), the graph shows they followed a similar trend to that previously observed for the base fluid and the base fluid and stabiliser mixture, and higher convective heat transfer coefficients were obtained for higher Reynolds number and temperatures, which was expected from the correlations. When comparing these values to those obtained for the pure base fluid (solid lines), an improvement in heat transfer performance in the nanofluid *versus* the base fluid was clearly noticeable on a constant Reynolds basis. This enhancement was greater for 140 °C and 200 °C, and more prominent for higher Reynolds numbers. As these temperatures came closer to the real working conditions of this HTF kind, a longer analysis had to be carried out for them.

The error analysis of the heat transfer coefficient was calculated as described in Ref. [46] and can be found in the Supporting Information. It gave average errors of 2.44% for the base fluid (TH66), 1.94% for the base fluid with OO (TH66 + OO) and 1.71% for the nanofluid (TH66 + OO + Sn). The errors obtained for the different convective heat transfer coefficient calculations done for the three studied fluids are found in the Supporting Information (Fig. S.4).

From the previously determined convective heat transfer coefficients, the improvement in nanofluid thermal performance was studied at higher temperatures: 140 °C and 200 °C. The results of this analysis are shown in Fig. 9, where the convective heat transfer coefficient enhancement of the nanofluid in relation to pure Therminol 66 and the Therminol 66 and OO mixture are depicted according to the Reynolds number studied in the experiments.

Fig. 9 shows how convective heat transfer coefficient enhancement tended to take a stable value for more turbulent regimes. At 200 °C, the maximum enhancements of 7.23% and 3.2% for the convective heat transfer coefficient of the nanofluid *vs.* the base fluid and the base fluid and OO mixture were predicted, with mean values of 5.99% and 1.73%, respectively. At 140 °C, enhancement was greater with improvements in
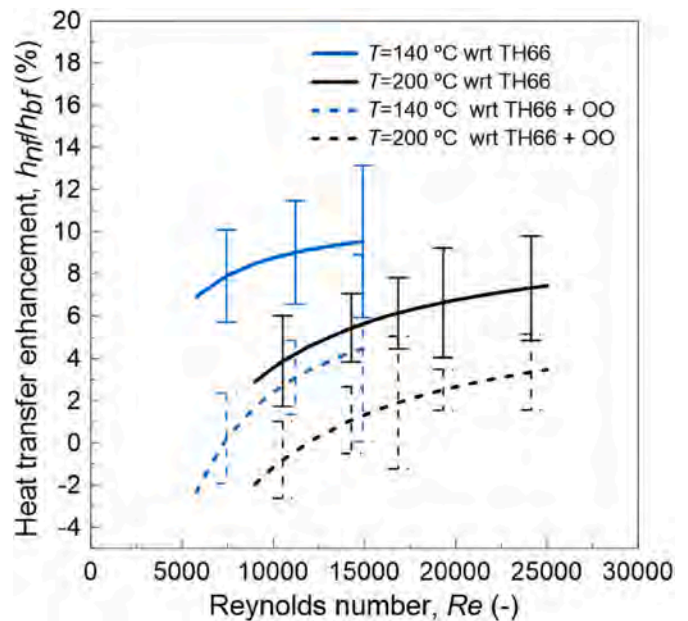

Fig. 9. Evolution of the convective heat transfer enhancement with Reynolds number for the nanofluid in relation to pure base fluid (TH66) and the base fluid with OO (TH66 + OO) at 140 °C and 200 °C.

the heat transfer capacity of up to 9.43% for the nanofluid in relation to the pure base fluid and 4.2% for the nanofluid *vs.* the base fluid and OO mixture with mean values of 8.55% and 1.87%, respectively.

The average errors obtained for the enhancement ratios of the convective heat transfer coefficients were 2.55% when comparing the nanofluid to Therminol 66 and 1.98% when comparing the nanofluid to Therminol 66 with OO.

The analysis was carried by taking into account the evolution of the heat transfer variables with Reynolds number. Heat transfer enhancement was obtained on a constant Reynolds basis. However, to ensure a constant Re when the working fluid changed from the base fluid to a nanofluid, the increase in viscosity needs to be compensated by a rise in the flow rate and, thus, in pumping power. Figs. S.5 and S.6 in the Supporting Information show the evolution of the heat transfer coefficient with flow rate, and a decrease when comparing values on a constant flow rate basis. Therefore, employing nanofluid as an HTF is beneficial when maintaining the Re value, but an agreement between the improved heat transfer and increased pumping power is needed.

5. Conclusions

An experimental setup for nanofluid heat transfer measurements taken at high temperature (up to 200 °C) was, to the best of the author's knowledge, done for the first time. The setup consists of a thermohydraulic loop that simulates the common working conditions for HTFs based on thermal oils. Given the relevance for the convective heat transfer coefficients of the temperature measurements taken in the loop, special care was taken during the calibration and correction processes. Three different fluids based on a commercial HTF, which were stabilised and characterised at high temperature in a previous work, were tested in the thermohydraulic loop: base fluid (TH66), base fluid and OO as a stabiliser and an Sn nanofluid based on TH66 + OO (1 wt%). A temperature range between 80 °C and 200 °C and a Reynolds number range from 2500 to 25,000 were modified at the experimental facility to evaluate the convective heat transfer coefficients of the three samples. The heat transfer coefficients measured in the loop showed good repeatability for the three measured fluids with differences below 3.6%. For the nanofluid (with differences below 1.7%), this good repeatability also indicated good nanofluid stability with time when operating in the thermohydraulic loop. Theoretical heat transfer coefficients were also calculated with two different Nusselt number correlations: Gnielinski and Ditus-Boelter. Using the thermo-physical properties measured experimentally instead of theoretical values led to a better consistency between the measured and theoretical Nusselt numbers and were, therefore, employed for all the calculations. Regarding the theoretical Nusselt correlation, that of Gnielinski better predicted the experimental results than that of Ditus-Boelter, and within a 15% deviation for Reynolds >5000. The repeatability study, as well as the comparison of the experimental data and the Nusselt theoretical correlations, confirmed and validated the accuracy of the results obtained by the thermohydraulic loop at high temperature. Albeit unusual in the bibliography, the obtained results confirmed that using experimental values of thermophysical properties for calculating convective heat transfer coefficients instead of theoretical correlations or models is very important to improve the accuracy of the results.

The employed nanofluid was generally able to enhance the convective heat transfer coefficient in relation to the base fluid, which tended to increase for higher studied temperatures (140 °C and 200 °C) and higher Reynolds numbers. As a result, enhancements up to 7.23% at 200 °C and 9.43% at 140 °C in the convective heat transfer coefficient can be achieved using the nanofluid (*vs.* the performance of the pure base fluid) for certain experimental conditions. These increases can play an important role to improve efficiencies and to cut the costs of many industrial applications that involve heat transfer, e.g. solar thermal energy sector, chemical or oil/gas industries, chemical reactors, etc.

Declaration of competing interest

The authors declare that they have no known competing financial interests or personal relationships that could have appeared to influence the work reported in this paper.

Data availability

Data will be made available on request.

Appendix A. Supplementary data

Supplementary data to this article can be found online at https://doi.org/10.1016/j.ijthermalsci.2021.107243.

References

[1] Grand View Research, Heat Transfer Fluids Market Size, Share & Trends Analysis Report by Application (Oil & Gas, Concentrated Solar Power), by Product (Aromatics, Glycols, Silicone), in: By Region, and Segment Forecasts, 2020 - 2027, 2020. San Francisco, CA, US.

[2] Frost & Sullivan, Next-Generation Fluid Formulations to Advance Global Heat Transfer Fluids Market toward $10 Billion by 2025, 2019.

[3] Z. Pavel, V. Vaclav, Various methods to improve heat transfer in exchangers, EPJ Web Conf. 92 (May 2015), 02119.

[4] K. Lunsford, Increasing heat exchanges performance, Hydrocarb. Eng. (1998) 55–61, 03 03.

[5] J. Sarkar, A critical review on convective heat transfer correlations of nanofluids, Renew. Sustain. Energy Rev. 15 (6) (2011) 3271–3277.

[6] M. Lomascolo, G. Colangelo, M. Milanese, A. De Risi, Review of heat transfer in nanofluids: conductive, convective and radiative experimental results, Renew. Sustain. Energy Rev. 43 (2015) 1182–1198.

[7] S.U.S. Choi, Enhancing thermal conductivity of fluids with nanoparticles, in: In American Society of Mechanical Engineers, Fluids Engineering Division (Publication) FED vol. 231, 1995, pp. 99–105.

[8] H. Masuda, A. Ebata, K. Teramae, N. Hishinuma, Alteration of thermal conductivity and viscosity of liquid by dispersing ultra-fine particles. Dispersion of Al2O3, SiO2 and TiO2 ultra-fine particles, Netsu Bussei 7 (4) (1993) 227–233.

[9] D. Wen, G. Lin, S. Vafaei, K. Zhang, Review of nanofluids for heat transfer applications, Particuology 7 (2) (2009) 141–150.

[10] N. Sezer, M.A. Atieh, M. Koç, A comprehensive review on synthesis, stability, thermophysical properties, and characterization of nanofluids, Powder Technol. 344 (Feb. 2019) 404–431.

[11] L. Qiu, et al., A review of recent advances in thermophysical properties at the nanoscale: from solid state to colloids, Phys. Rep. 843 (2020) 1–81.

[12] M.H. Buschmann, et al., Correct interpretation of nanofluid convective heat transfer, Int. J. Therm. Sci. 129 (June 2017) (2018) 504–531.

[13] W. Yu, E.V. Timofeeva, D. Singh, D.M. France, R.K. Smith, Investigations of heat transfer of copper-in-Therminol 59 nanofluids, Int. J. Heat Mass Tran. 64 (1) (2013) 1196–1204.

[14] A.A. Minea, M.G. Moldoveanu, Studies on Al2O3, CuO, and TiO2 water-based nanofluids: a comparative approach in laminar and turbulent flow, J. Eng. Thermophys. 26 (2) (2017) 291–301.

[15] B. Raei, F. Shahraki, M. Jamialahmadi, Experimental study on the heat transfer and flow properties of c -Al 2 O 3/water nanofluid in a double-tube heat exchanger, J. Therm. Anal. Calorim. 127 (3) (2017) 2561–2575.

[16] W. Williams, J. Buongiorno, L.-W. Hu, Experimental investigation of turbulent convective heat transfer and pressure loss of alumina/water and zirconia/water nanoparticle colloids (nanofluids) in horizontal tubes, J. Heat Tran. 130 (4) (Apr. 2008) 1–7.

[17] V. Mikkola, S. Puupponen, H. Granbohm, K. Saari, T. Ala-Nissila, A. Seppälä, Influence of particle properties on convective heat transfer of nanofluids, Int. J. Therm. Sci. 124 (October 2017) (Feb. 2018) 187–195.

[18] A.E. Kabeel, M. Abdelgaied, "Overall heat transfer coefficient and pressure drop in a typical tubular exchanger employing alumina nano - fluid as the tube side hot fluid, Heat Mass Tran. 52 (8) (2016) 1417–1424.

[19] R. Martínez-Cuenca, et al., Forced-convective heat-transfer coefficient and pressure drop of water-based nanofluids in a horizontal pipe, Appl. Therm. Eng. 98 (2016) 841–849.

[20] N. Nikkam, et al., "Experimental study on preparation and base liquid effect on thermo-physical and heat transport characteristics of α -SiC nano fl uids ☆, Int. Commun. Heat Mass Tran. 55 (2014) 38–44.

[21] K.S. Suganthi, V.L. Vinodhan, K.S. Rajan, "Heat transfer performance and transport properties of ZnO – ethylene glycol and ZnO – ethylene glycol – water nanofluid coolants 135 (2014) 548–559.

[22] M.M. Sarafraz, F. Hormozi, Intensification of forced convection heat transfer using biological nanofluid in a double-pipe heat exchanger, Exp. Therm. Fluid Sci. 66 (Sep. 2015) 279–289.

[23] R.S. Vajjha, D.K. Das, D.P. Kulkarni, Development of new correlations for convective heat transfer and friction factor in turbulent regime for nanofluids, Int. J. Heat Mass Tran. 53 (21–22) (Oct. 2010) 4607–4618.

[24] A. Zamzamian, S.N. Oskouie, A. Doosthoseini, A. Joneidi, M. Pazouki, Experimental investigation of forced convective heat transfer coefficient in nanofluids of Al2O3/EG and CuO/EG in a double pipe and plate heat exchangers under turbulent flow, Exp. Therm. Fluid Sci. 35 (3) (Apr. 2011) 495–502.

[25] J. Pérez-Tavernier, J.P. Vallejo, D. Cabaleiro, J. Fernández-Seara, L. Lugo, Heat transfer performance of a nano-enhanced propylene glycol:water mixture, Int. J. Therm. Sci. 139 (February) (May 2019) 413–423.

[26] A. Asadi, et al., Recent advances in preparation methods and thermophysical properties of oil-based nanofluids: a state-of-the-art review, Powder Technol. 352 (2019) 209–226.

[27] P. Razi, M.A. Akhavan-Behabadi, M. Saeedinia, Pressure drop and thermal characteristics of CuO-base oil nanofluid laminar flow in flattened tubes under constant heat flux, Int. Commun. Heat Mass Tran. 38 (7) (2011) 964–971.

[28] M. Saeedinia, M.A. Akhavan-Behabadi, P. Razi, Thermal and rheological characteristics of CuO-Base oil nanofluid flow inside a circular tube, Int. Commun. Heat Mass Tran. 39 (1) (2012) 152–159.

[29] A. Naddaf, S. Zeinali, B. Pouladi, An experimental study on heat transfer performance and pressure drop of nano fl uids using graphene and multi-walled carbon nanotubes based on diesel oil, Powder Technol. 352 (2019) 369–380.

[30] B.-H. Chun, H.U. Kang, S.H. Kim, Effect of alumina nanoparticles in the fluid on heat transfer in double-pipe heat exchanger system, Kor. J. Chem. Eng. 25 (5) (Sep. 2008) 966–971.

[31] A. Amiri, et al., Laminar convective heat transfer of hexylamine-treated MWCNTs-based turbine oil nanofluid, Energy Convers. Manag. 105 (2015) 355–367.

[32] S.Z. Heris, F. Farzin, H. Sardarabadi, Experimental comparison among thermal characteristics of three metal oxide nanoparticles/turbine oil-based nanofluids under laminar flow regime, Int. J. Thermophys. 36 (4) (2015) 760–782.

[33] Y. Yang, Z.G. Zhang, E.A. Grulke, W.B. Anderson, G. Wu, Heat transfer properties of nanoparticle-in-fluid dispersions (nanofluids) in laminar flow, Int. J. Heat Mass Tran. 48 (6) (Mar. 2005) 1107–1116.

[34] M.M. Derakhshan, S.G. Mohseni, "Experiments on mixed convection heat transfer and performance evaluation of MWCNT – oil nanofluid flow in horizontal and vertical microfin tubes, Exp. Therm. Fluid Sci. 61 (2015) 241–248.

[35] M. Fakoor Pakdaman, M.A. Akhavan-Behabadi, P. Razi, An experimental investigation on thermo-physical properties and overall performance of MWCNT/ heat transfer oil nanofluid flow inside vertical helically coiled tubes, Exp. Therm. Fluid Sci. 40 (Jul. 2012) 103–111.

[36] F. Farzin, S.Z. Heris, S. Rahimi, Laminar convective heat transfer and pressure drop of Tio 2/turbine oil nanofluid, J. Thermophys. Heat Tran. 27 (1) (2013) 127–133.

[37] U. Srivastva, R.K. Malhotra, S.C. Kaushik, Experimental investigation of convective heat transfer properties of synthetic fluid, J. Therm. Anal. Calorim. 132 (1) (Apr. 2018) 709–724.

[38] B.D. Gajbhiye, S.C. S, C.S. Mathpati, A.W. Patwardhan, A. Borgohain, N. K. Maheshwari, Pretest in forced circulation molten salt heat transfer loop: studies with thermia-B, Heat Tran. Res. 48 (8) (Dec. 2019) 4354–4372.

[39] J. Lu, X. Sheng, J. Ding, J. Yang, Transition and turbulent convective heat transfer of molten salt in spirally grooved tube, Exp. Therm. Fluid Sci. 47 (2013) 180–185.

[40] C. Chen, Y. Wu, S. Wang, C. Ma, Experimental investigation on enhanced heat transfer in transversally corrugated tube with molten salt, Exp. Therm. Fluid Sci. 47 (2013) 108–116.

[41] J. Lu, S. He, J. Liang, J. Ding, J. Yang, Convective heat transfer in the laminar-turbulent transition region of molten salt in annular passage, Exp. Therm. Fluid Sci. 51 (2013) 71–76.

[42] W. Yu-ting, L. Bin, M. Chong-fang, G. Hang, Convective heat transfer in the laminar-turbulent transition region with molten salt in a circular tube, Exp. Therm. Fluid Sci. 33 (7) (2009) 1128–1132.

[43] H.W. Hoffman, S.I. Cohen, Fused Salt Heat Transfer-Ppart III: Forced-Convection Heat Transfer in Circular Tubes Containing the Salt Mixture NaNO2-NaNO3-KNO3, Mar. 1960. Oak Ridge, TN (United States).

[44] S.M.S. Murshed, P. Estellé, A state of the art review on viscosity of nanofluids, Renew. Sustain. Energy Rev. 76 (August 2016) (2017) 1134–1152.

[45] J. Gil-Font, et al., Improving heat transfer of stabilised thermal oil-based tin nanofluids using biosurfactant and molecular layer deposition, Appl. Therm. Eng. 178 (Sep. 2020) 115559.

[46] J.E. Julia, et al., Measurement and modelling of forced convective heat transfer coefficient and pressure drop of Al 2 O 3 - and SiO 2 -water nanofluids, J. Phys. Conf. Ser. 395 (1) (Nov. 2012) 012038.

[47] W. Yu, D.M. France, D.S. Smith, D. Singh, E.V. Timofeeva, J.L. Routbort, Heat transfer to a silicon carbide/water nanofluid, Int. J. Heat Mass Tran. 52 (15–16) (Jul. 2009) 3606–3612.

[48] V. Gnielinski, On heat transfer in tubes, Int. J. Heat Mass Tran. 63 (2013) 134–140.

[49] [Online]. Available: Therminol 66 Data Sheet https://www.therminol.com/sites/t herminol/files/documents/TF-8695_Therminol-66_Technical_Bulletin.pdf.